Cell Reports, Volume *42*

Supplemental information

Data-driven multiscale model of macaque auditory thalamocortical circuits reproduces *in vivo* dynamics

Salvador Dura-Bernal, Erica Y. Griffith, Annamaria Barczak, Monica N. O'Connell, Tammy McGinnis, Joao V.S. Moreira, Charles E. Schroeder, William W. Lytton, Peter Lakatos, and Samuel A. Neymotin

Supplemental Information

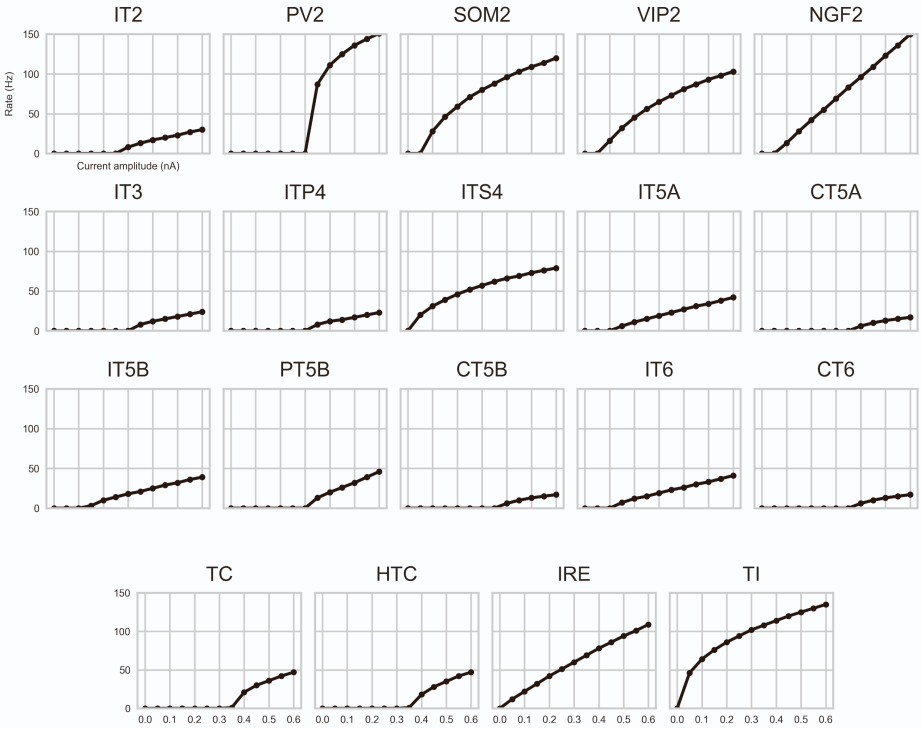

S1. Frequency-current (f-I) curves of all distinct cortical and thalamic cell types used in the model. X-axis shows the amplitude of somatic current injection provided over a 1 second interval, and y-axis shows the number of action potentials produced.

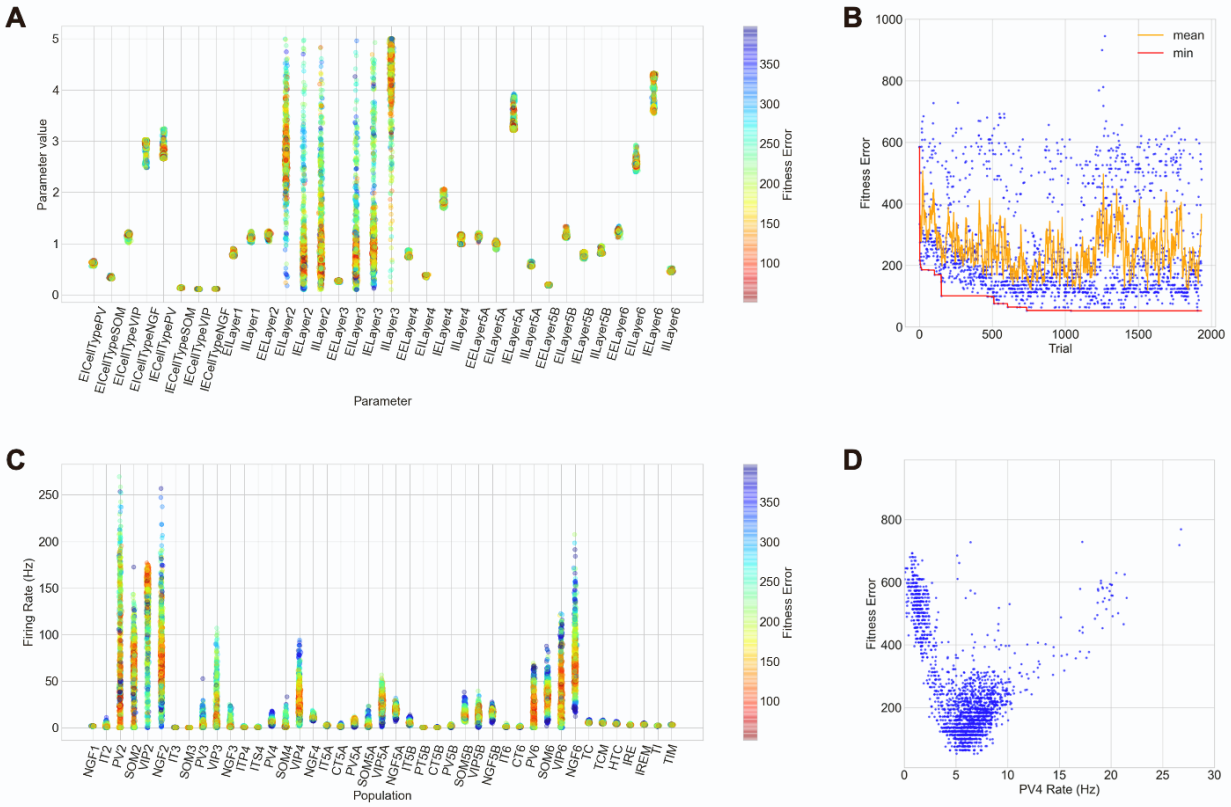

S2. Optimization of connectivity parameters in auditory thalamocortical model. A) Range of values explored for each parameter tuned, and fitness error (color) associated with each value. Only parameter values with fitness errors below 400 were included; red indicates the approximate final parameter value. Note that only layer 2 and 3 connectivity parameters were tuned across a wide value range, while the rest of parameters were highly constrained based on previous optimizations. B) Fitness error of the trials, each evaluating a different parameter combination; moving mean average across 10 trials (orange); overall minimum fitness (red) shows fast improvement up to ~750 trials and then plateaus. C) Range of average firing rates obtained for each population, and fitness error (color) associated with each value. Only rates with fitness errors below 400 were included; red indicates the approximate final rate. D) Relation between fitness error and PV4 average firing rate; the V-shape indicates very low or very high firing rates were correlated with high fitness errors, whereas firing rates close to the target (~5-10 Hz) were correlated with low fitness error.

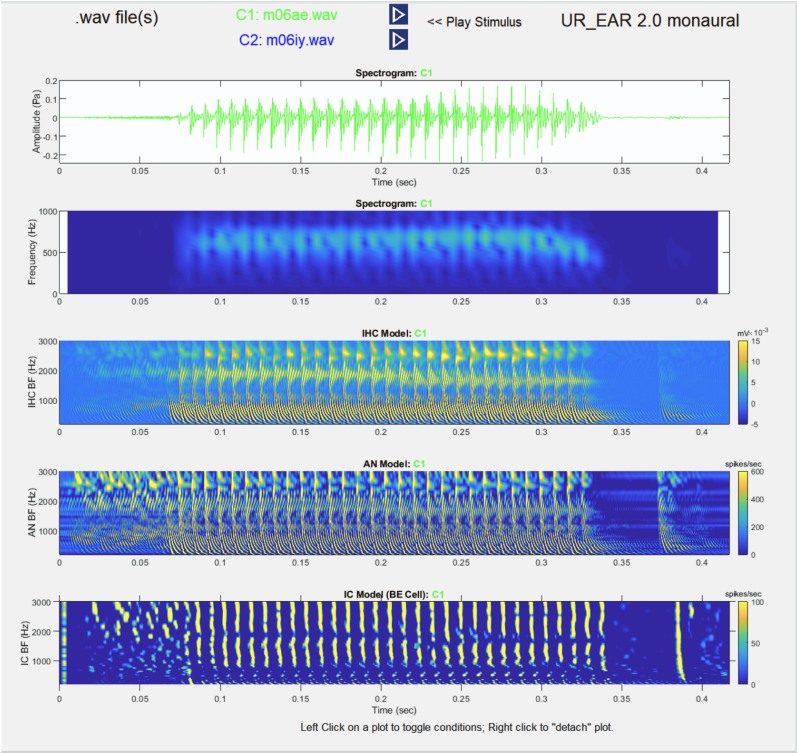

S3. Example output of the cochlea and inferior colliculus (IC) phenomenological model. From top to bottom: time series of example input sound (.wav file); spectrogram of the input sound; output of the Cochlear inner hair cells (IHC) model (in mV); output of the auditory nerve (AN) model (in Hz); output of the IC model (in mV). The firing rates of the IC units are then converted to spike times and provided as input to the biophysically detailed MGB model.

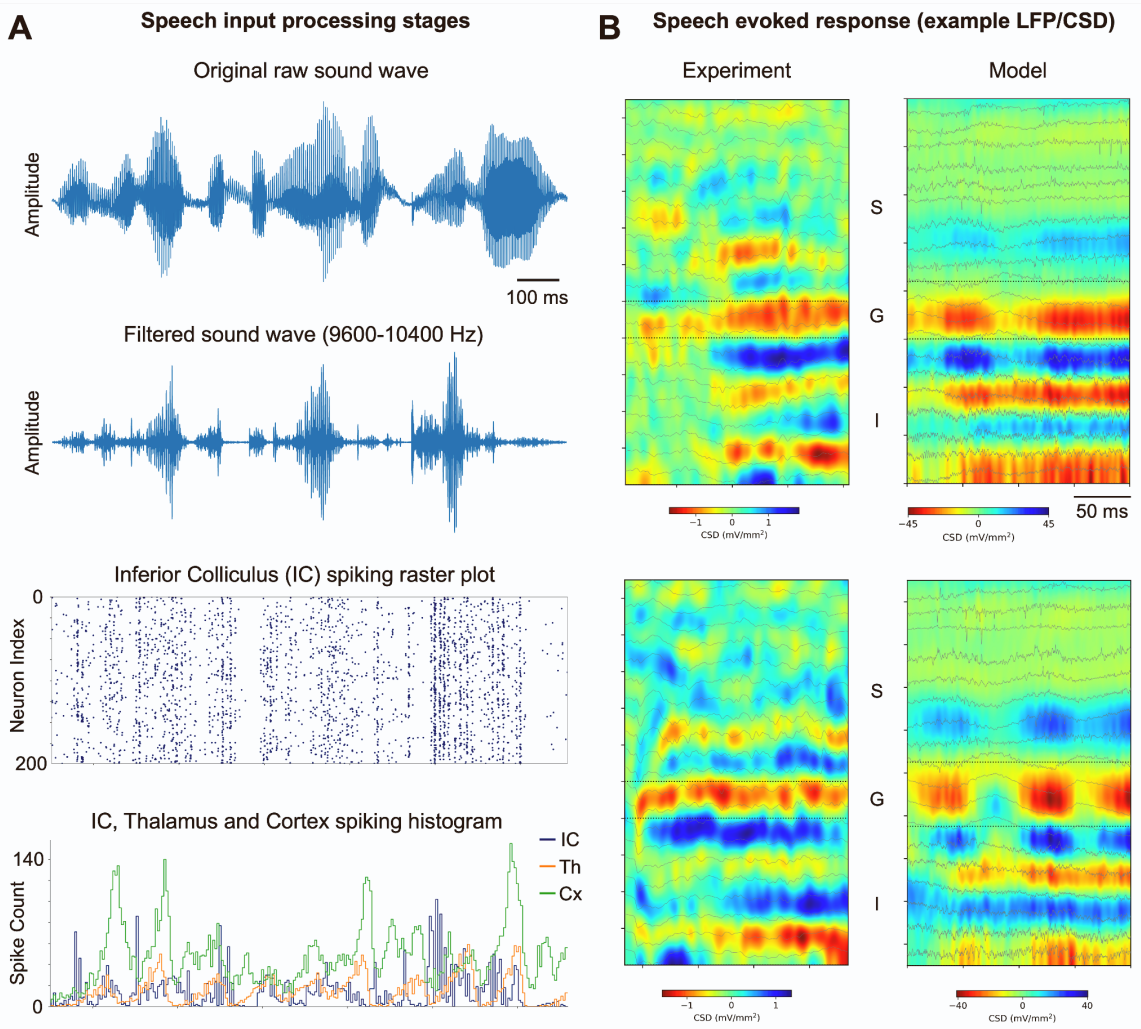

S4. Model processing stages for speech input and comparison of example laminar LFP/CSD for macaque vs model. A) Speech input sound processing stages (top to bottom): raw sound wave ("Would you like a banana Peter ?"); filtered sound wave based on auditory cortex center frequency (9600 to 10400 Hz); spiking response of model inferior colliculus (IC) based on AC/IC phenomenological model instantaneous firing rates; and spiking histogram of IC, thalamus and cortex in response to speech input. **B)** Example LFP/CSD model responses exhibited features comparable to those recorded in macaque, for example, ~150-200ms long current sinks in the granular layer, with alternating current sources and sinks in the infragranular layers. These preliminary results primarily serve to illustrate how the cochlea and IC model can be used to provide auditory stimuli to the biophysical thalamocortical model, which in turn generates LFP/CSD activity patterns that can be directly compared to experimental data. However, the model has not yet been tuned or systematically validated to reproduce the complex responses evoked by speech inputs. Transmembrane currents (sinks and sources) in CSD color maps are color-coded red and blue, respectively. Y-axis represents LFP and related CSD channels at depths spanning pia to white matter, with supragranular (S), granular (G) and infragranular (I) layers indicated.

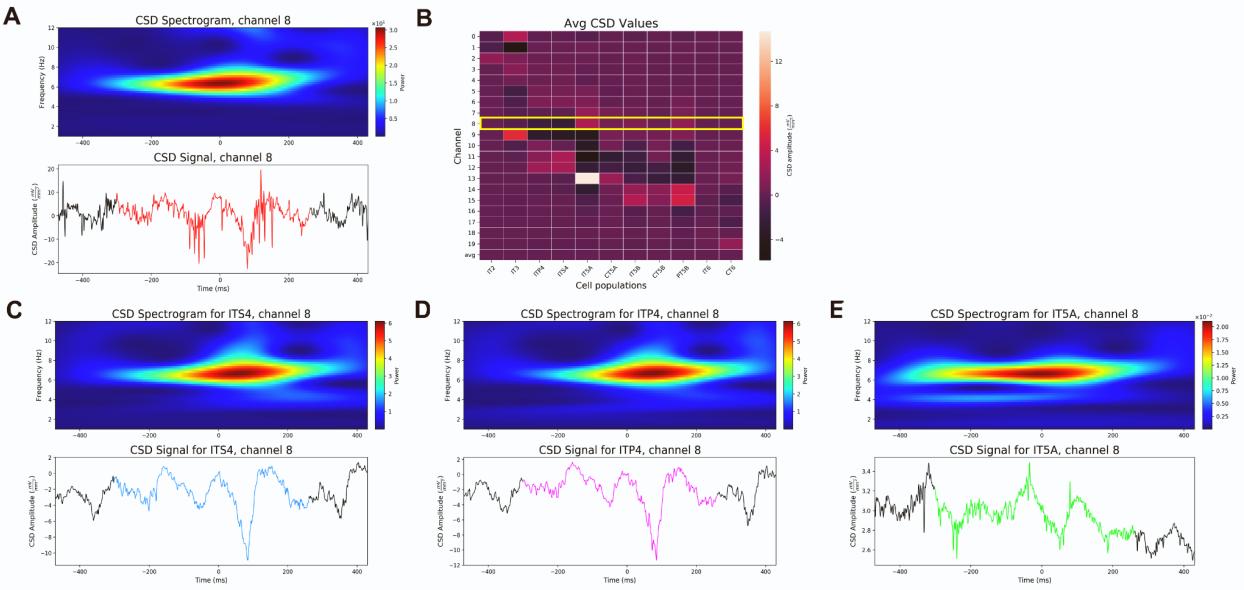

Figure S5. Model predicts layer- and cell type-specific sources of LFP/CSD during oscillations. A) CSD reveals a theta oscillation in A1 supragranular layer (see Fig. 6). **B)** Heat map depicting the average CSD amplitude (mV/mm^2) during the time of the theta oscillation event across excitatory model populations and channels. The CSD spectrogram and time series (top panels*)* and the firing rate spectrogram and histogram (bottom panels) of the 3 populations with the strongest contributions to the theta oscillation depicted in **(A)** are shown in **(C)** ITS4, **(D)** ITP4, and **(E)** IT5A.